Inorganic Chemistry
Cite This: Inorg. Chem. 2018, 57, 4891−4897
Article
pubs.acs.org/IC

Incorporation of In_2S_3 Nanoparticles into a Metal−Organic Framework for Ultrafast Removal of Hg from Water

Linfeng Liang,[†,‡] Luyao Liu,[‡] Feilong Jiang,[‡] Caiping Liu,[‡] Daqiang Yuan,[‡] Qihui Chen,*[,‡] Dong Wu,[†,‡] Hai-Long Jiang,*[,†] and Maochun Hong*[,†,‡]

[†]Department of Chemistry, University of Science and Technology of China, Hefei, Anhui 230026, People's Republic of China
[‡]State Key Laboratory of Structural Chemistry, Fujian Institute of Research on the Structure of Matter, Chinese Academy of Sciences, Fuzhou 350002, People's Republic of China

Supporting Information

ABSTRACT: Considering rapidly rising Hg emission from industrial waste effluents, it is imperative to explore practical and effective adsorbents for Hg. Herein, a mild and facile method has been developed to confine ultrasmall In_2S_3 nanoparticles (about 2.5 nm) in the cavities of a MOF for the first time. The resulting composite (In_2S_3@MIL-101) can remove 99.95% of the Hg^{2+} from wastewater very efficiently in as short as 1 min with the highest distribution coefficient (2.2×10^7 mL g^{-1}) among all MOF-based mercury adsorbents. It also displays excellent selectivity for Hg even when other interferential metal ions are present, and it can be reused with almost retained adsorption capacity. All of these features make the composite a potential adsorbent for Hg removal from industrial wastewater.

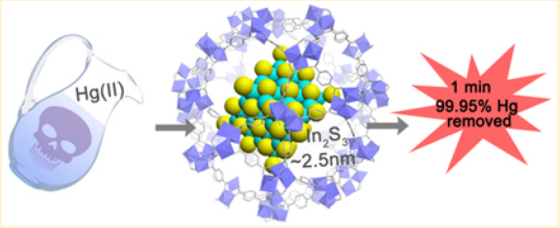

1. INTRODUCTION

Among the heavy-metal pollutants, the pollution from mercury (Hg) represents a major concern, as it can cause various diseases in humans and animals and poses a threat to public health and the environment.[1] Release of mercury into the environment is mainly through the production of industrial products and byproducts, such as batteries, plastic products, various chemicals, and so on.[2,3] Even though the WHO has been strongly trying to raise awareness to reduce the amount of Hg in domestic tools and in different industrial sectors, the world's annual Hg consumption is still estimated as being up to 2000 tons in 2016.[2] Therefore, the efficient removal of Hg from industrial waste effluents is highly urgent. In comparison with traditional precipitation methods, adsorption methods using porous materials are among the most promising methods in wastewater treatment and the remediation of a contaminated environment due to its simplicity and low cost. Conventional adsorbents such as carbon materials, polymers, and clays have been thoroughly investigated in the removal of Hg.[4−7] However, these materials usually face challenges such as low mercury uptake amount, poor selectivity, weak binding affinity, slow kinetics, etc. Hence, it is imperative to explore more practical and effective adsorbents that can remove Hg from industrial waste effluents selectively and rapidly.

Metal−organic frameworks (MOFs) are very promising kinds of highly porous and crystallized materials, and they have been applied in many fields such as catalysis, selective gas storage and separation, fluorescence detection, etc. due to their properties such as high crystallinity, permanent porosity, extraordinarily high surface areas, and easily functionlized pore surface.[8−33] Their easily accessible pore surface and evenly distributed functional sites that can be introduced purposefully make heavy metal ion adsorption possible.[34−46] Since a methylthio group first combined with MOFs to adsorb Hg(II) by the Xu group,[34] different kinds of functional groups have been combined with MOFs to catch Hg(II) through Hg−S interactions or Hg−N interactions.[2,47−53] Indeed, by introduction of thio-/thiol-functionalized groups into their backbones, MOFs have been proved to be particularly efficient sorbents for Hg(II). Nevertheless, the harsh conditions and expensive reagents needed for the introduction of organic sulfur functional groups significantly restrict their practical application. To solve the aforementioned problems, a new strategy has been developed for sulfur functionalization of MOFs by incorporation of inorganic ultrasmall metal sulfide nanoparticles (NPs), which can interact with Hg ions through their large amount of exposed S atoms on the surface for efficient Hg removal (Scheme 1).

2. EXPERIMENTAL SECTION

2.1. Materials and Methods. All chemicals were used as purchased from commercial sources without further purification: chromium(III) nitrate nonahydrate ($Cr(NO_3)_3{\cdot}9H_2O$, Sigma-Aldrich, 99%,), benzene-1,4-dicarboxylic acid (TCI, > 99.0%), NH_4F (Energy Chemical, 98%), and aqueous HF (Aladdin Industrial Inc., 40%). Deionized water was prepared with a set of Master-Q30UT equipment with a specific resistance of 18.25 MΩ cm. The concentrations of mercury were determined by using a JY ULTIMA 2 ICP instrument and BJHG AFS-230E atomic fluorescence spectrometer. The powder X-ray diffraction patterns (PXRD) were collected by a Rigaku D

Received: December 6, 2017
Published: April 25, 2018

ACS Publications © 2018 American Chemical Society

DOI: 10.1021/acs.inorgchem.7b03076
Inorg. Chem. 2018, 57, 4891−4897

Scheme 1. Illustration Showing the Preparation of In_2S_3 NPs inside MIL-101 for Efficient Hg Removal from Water

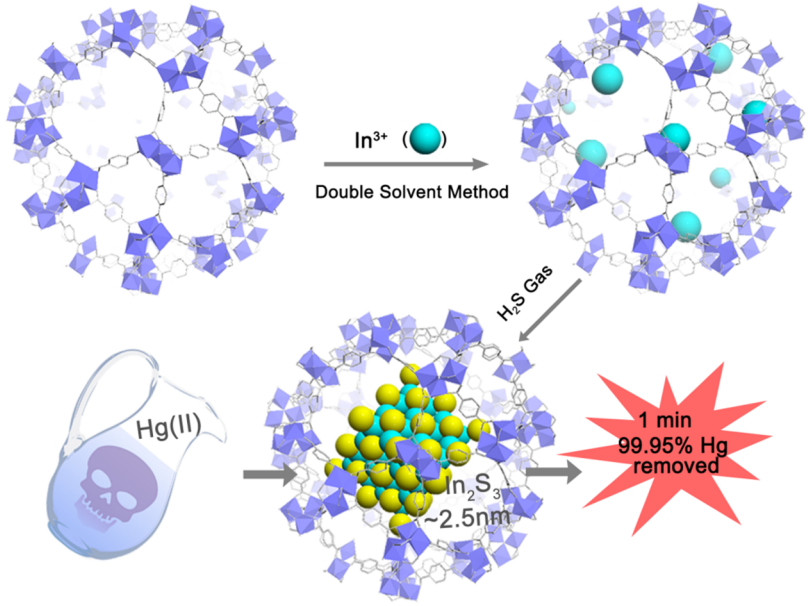

instrument using Cu Kα radiation (λ = 0.154 nm) at room temperature. Single-component gas adsorption measurements were performed with the ASAP2020 System (Micromeritics). Transmission electron microscopy (TEM), high-angle annular dark-field scanning transmission electron microscopy (HAADF-STEM), and elemental mapping were carried out on a FEIT 20 transmission electron microscope (TEM) working at 200 kV. X-ray photoelectron spectroscopy (XPS) was performed on an ESCALAB 250Xi system to determine the surface electronic state of the composite.

2.2. Synthetic Procedures. *2.2.1. Preparation of MIL-101.* MIL-101 powder was obatined through a hydrothermal reaction. A mixture of terephthalic acid (332 mg, 2.0 mmol), $Cr(NO_3)_3{\cdot}9H_2O$ (800 mg, 2.0 mmol), and HF solution (0.1 mL, 0.5 mmol) was dissolved in 9.5 mL of deionized water and reacted in a 200 °C oven for 8 h. MIL-101 was refluxed in water for 12 h and refluxed in ethanol twice for 1 day, and finally refluxed one time in NH_4F solution. The MIL-101 obtained after purification was further subjected to vacuum overnight at 150 °C before use.

2.2.2. Preparation of In^{3+}@MIL-101. MIL-101 (200 mg) was dispersed in dry *n*-hexane (40 mL) and sonicated for about 20 min. Aqueous $In(NO_3)_3$ solution (1 M, 0.32 mL) was added with constant stirring with a speed of 10 μL min^{-1} using a syringe pump. Subsequently, the mixture was further stirred for 8 h. Finally, the solid could be obtained simply by decanting the supernatant and drying it naturally at room temperature. The obtained solid was further dried under vacuum conditions for 1/2 day.

2.2.3. Preparation of In_2S_3@MIL-101. The In^{3+}@MIL-101 sample obtained above was packed on an apparatus as depicted in Figure S1 to conduct a solid−gas reaction with H_2S gas. Typically, 10 mL of formic acid was placed in a conical flask loaded with 10 g of Na_2S to generate H_2S gas. Subsequently, the resultant solid was continuously immersed under H_2S conditions for another 12 h. The obtained product was further treated at 50 °C in a vacuum box for 12 h.

3. RESULTS AND DISCUSSION

3.1. Preparation and Characterization of In_2S_3@MIL-101. Considering the extraordinarily high surface area, large pore volume, and exceptional water and chemical stability, a representative MOF, MIL-101 (Cr),[54] was selected to incorporate water-stable In_2S_3 NPs (K_{sp} values as high as 5.7×10^{-74}). To implant In_2S_3 NPs into the open cavities of MIL-101, In^{3+} was first introduced via a double-solvent method[55] followed by a solid−gas reaction with hydrogen sulfide. The synthesis progress was monitored by the color evolution of the solid (Figure S2), and the change was determined by TEM, HAADF-STEM, and elemental mapping analyses (Figure 1a−d). Elemental mapping (Figure 1d) indicates that S and In species are dispersed uniformly throughout the MIL-101 matrix (Figure 1d), implying the formation of In_2S_3 NPs. As shown in Figure 1a−c, the average size of the In_2S_3 NPs is about 2.5 nm, which is slightly smaller than the cavity of MIL-101, revealing the confinement of its large cavities. PXRD studies also prove the appearance of In_2S_3 species. As is shown in Figure 1e, the peaks located at 2θ = 27.5, 33.4, and 47.9° are distinctly indexed to the (311), (400), and (440) crystal planes of the β-In_2S_3 phase structure (In_2S_3) (JCPDS 32-0456). The preservation of structural integrity for MIL-101 after the introduction of In_2S_3 has also been verified by the consistence in the PXRD patterns of In_2S_3@MIL-101, while the relative diffraction intensity decreases between 2θ = 4 and 6°, and this can be interpreted by the significant occupancy of the pore space region (i.e., the system becomes less porous) because of the incorporation of In_2S_3 NPs. Additionally, according to the XPS spectra of Cr 2p regions shown in Figure S3, the binding energy of Cr 2p regions of In_2S_3@MIL-101 is the same as that in pure MIL-101, confirming the invariability of the valence and surrounding environment of Cr(III). Particularly, bulk In_2S_3@MIL-101 can be facilely synthesized even on a 10 g scale (for more details see section S1 in the Supporting Information), making its practical application possible.

The porosity of In_2S_3@MIL-101 was analyzed by N_2 sorption tests and compared with that of MIL-101 (Figure 1f). As we expected, an obvious Brunauer−Emmett−Teller (BET) surface area decrease is observed, from 3026 m^2/g (MIL-101) to 1476 m^2/g (In_2S_3@MIL-101). This significant decrease should be caused by more a than mass increase when the loading amount of In_2S_3 is 26% (m/m). In the meantime, the pore volume decreases from 1.70 mL/g (MIL-101) to 0.76 mL/g (In_2S_3@MIL-101), and this is also not only due to the mass increase. The pore size distributions of MIL-101 and In_2S_3@MIL-101 indicate that the pore size becomes smaller after introduction of In_2S_3 nanoparticles into MIL-101 (Figure

DOI: 10.1021/acs.inorgchem.7b03076
Inorg. Chem. 2018, 57, 4891−4897

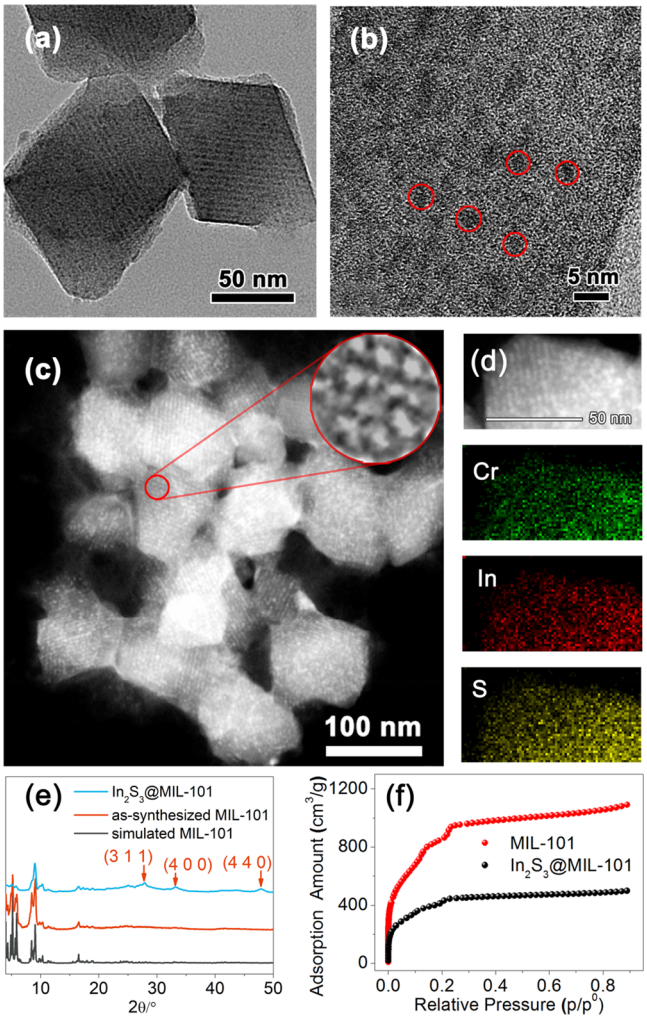

Figure 1. (a, b) TEM and (c) HAADF-STEM images of In_2S_3@MIL-101. (d) TEM image and corresponding elemental mapping of the Cr, In, and S atoms for the selected area (marked with red rectangle). (e) PXRD patterns and (f) N_2 sorption isotherms at 77 K for different samples.

S4). Therefore, In_2S_3 should be incorporated inside MIL-101, leading to the decrease in pore size and surface area.

3.2. Hg Adsorption Isotherms. An ideal and practical adsorbent for Hg from industrial waste effluents should display the following advantages: (1) fast adsorption kinetics, (2) large adsorption capacity, (3) high selectivity with interferential heavy-metal ions, (4) excellent capacity in an acid enviromnent, and (5) good reusability and ready large-scale preparation. Therefore, a series of tests were carried out to estimate the Hg adsorption capacity of In_2S_3@MIL-101 (section S2 in the Supporting Information). The data for the Hg adsorption isotherms were obtained from Hg solutions with different initial concentrations (10−1000 mg L^{-1}) at pH 7 (Figure 2a). The Langmuir adsorption isotherm model and the Freundlich adsorption isotherm model were used to fit the experimental adsorption isotherm data (Figure 2b and Figure S6). The calculated correlation coefficient and linear regression coefficient (R^2) values for both the two models are given in Table S1. In the case of the R^2 values, the Freundlich model generated a more suitable fit to the obtained data in comparison to the Langmuir model with an R^2 value greater than 0.991, conforming to the fact that the inner surface of In_2S_3@MIL101 was more heterogeneous.[56−59] In the meantime, In_2S_3@MIL-101 gave a maximum adsorption amount of 518.2 mg g^{-1} with an initial Hg concentration of 1000 mg L^{-1}. Although the capacity is lower than that of $Ca^{II}Cu^{II}_6[(S,S)\text{-methox}]_3(OH)_2(H_2O)\}$ (900 mg g^{-1})[2] and $[Cu_3(BTC)_2]$-SH (714.29 mg g^{-1}),[60] it surpasses those of almost all MOF adsorbent materials such as Zr-DMBD (197 mg g^{-1}),[48] Zr-M1 (275 mg g^{-1}),[52] Zn(hip)(L)(DMF)(H_2O) (333 mg g^{-1}),[51] FJI-H12 (440 mg g^{-1}),[50] MFC-S (282 mg g^{-1}),[61] and Fe_3O_4@SiO_2@HKUST-1 (264 mg g^{-1}),[62] highlighting its potential for application in wastewater treatment. Moreover, its adsorption capacity is also higher than that of many famous sulfur-containing porous materials, such as KMS-1 (377 mg g^{-1})[63] and LHMS-1 (91 mg g^{-1}),[64] which could be attributed to the large amounts of exposed S atoms of In_2S_3 NPs distributed throughout the pores of MIL-101.

3.3. Kinetics of Hg Adsorption and Proposed Adsorption Mechanism. Since the capture of Hg from wastewater is usually carried out in a fixed-bed reactor, the adsorption kinetics is a very important parameter for practical application. The kinetics was evaluated at an initial mercury concentration of 10 ppm at pH 7. As shown in Figure 2c and the inset, an extremely fast kinetics is observed for In_2S_3@MIL-101, which can remove 99.95% of the mercury ions in as short as 1 min. Even though the initial mercury concentration is as low as 10 ppm, In_2S_3@MIL-101 can reduce the Hg(II) concentration down to 1.75 ppb, which is lower than the drinking water limit of 2 ppb. The experimental data were then fitted with the pseudo-second-order kinetic model using the equation

$$\frac{t}{q_t} = \frac{1}{k_2 q_e^2} + \frac{t}{q_e}$$

where q_t (mg g^{-1}) represents the Hg adsorption amount at time t (min) and q_e (mg g^{-1}) that at equilibrium. The parameter k_2 (g mg^{-1} min^{-1}) is an adsorption rate constant (Figure 2d). A very high correlation coefficient (>0.9999) was determined, suggesting that the current model was appropriate for the adsorption kinetics. The value of k_2 was calculated to be 2.02 g mg^{-1} min^{-1}, which much higher than those of traditional materials under similar conditions.[65−67] Except for the large cavity of MIL-101 which could promote rapid mass diffusion and transport, such extraordinary fast kinetics also indicated a high affinity between Hg and In_2S_3@MIL-101, and this was further demonstrated by XPS tests. As shown in Figure 2e,f and Figure S3, when In_2S_3@MIL-101 is compared before and after Hg adsorption, a dramatic change in S 2p binding energy is observed, from 162.1 to 163.2 eV, while the XPS spectra of In 3d and Cr 2p spectra were the same as that in In_2S_3@MIL-101, suggesting that the Hg interacted with the adsorbent mainly through exposed S atoms of the In_2S_3 NPs. The distribution coefficient (K_d) value of the hybrid sample In_2S_3@MIL-101 for Hg adsorption was calculated to be 2.2×10^7 mL g^{-1} (section S2 in the Supporting Information), which is the highest among all reported MOF-based mercury adsorbents, such as Zr-DMBD (9.99×10^5 mL g^{-1}),[48] $[Cu_3(BTC)_2]$-SH (4.73×10^5 mL g^{-1}),[60] Zr-M1 (1.47×10^4 mL g^{-1}),[52] Zn-hip (1.11×10^6 mL g^{-1}),[51] FJI-H12 (1.86×10^6 mL g^{-1}),[50] $Zn_4O(L)_3$ (3.16×10^3 mL g^{-1}),[47] LMOF-263 (6.45×10^5 mL g^{-1}),[53] and $Cu_6Ca[(S,S)\text{-methox}]_3(OH)_2(H_2O)\cdot 16H_2O$ (6.67×10^5 mL g^{-1}).[2] Moreover, such a high K_d is comparable to that of the famous PAF-1-SH (5.76×10^7 mL g^{-1})[68] and exceeds those of

DOI: 10.1021/acs.inorgchem.7b03076
Inorg. Chem. 2018, 57, 4891−4897

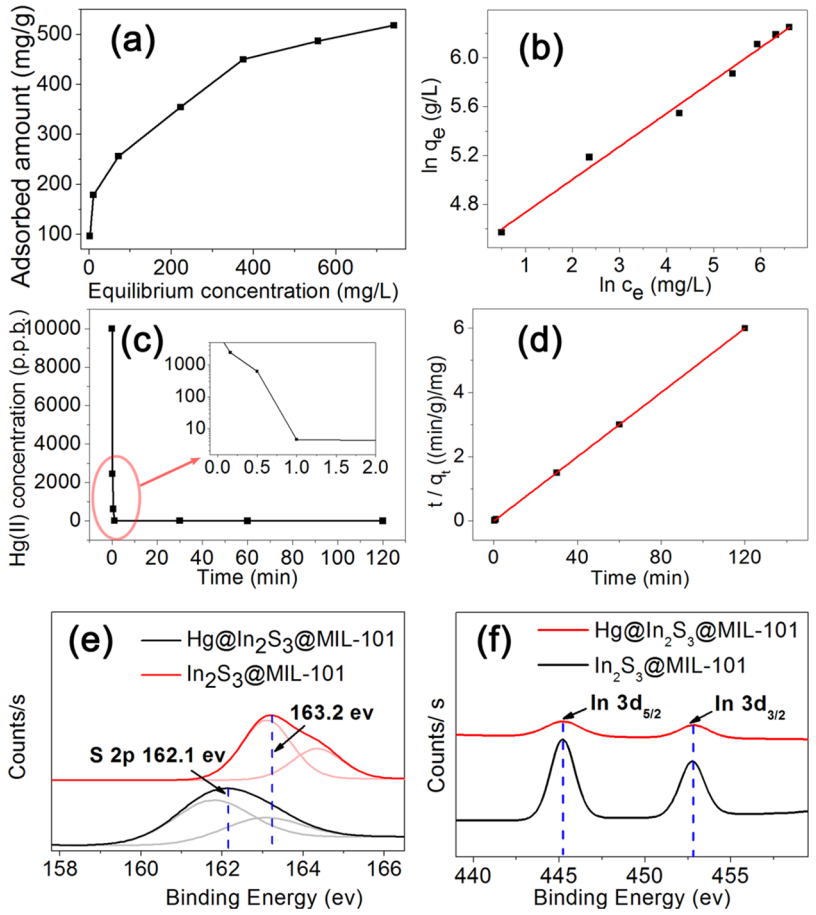

Figure 2. (a) Hg adsorption isotherm for In_2S_3@MIL-101. (b) Freundlich fitting for the adsorption of mercury onto In_2S_3@MIL-101. (c) Hg(II) sorption kinetics of In_2S_3@MIL-101 at an Hg(II) initial concentration of 10 ppm. The inset shows the adsorption kinetics enlarged in a range from 0 to 2 min. (d) Pseudo-second-order models for the adsorption of mercury onto In_2S_3@MIL-101. (e) S 2p and (f) In 3d XPS spectrum comparison (the four peaks in light colors in (e) originate from the S 2p spin orbital splitting).

many other famous sulfur-containing porous materials such as TAPB-BMTTPA-COF (7.82×10^5 mL g^{-1}),[69] sulfide-modified mesoporous carbon (6.82×10^5 mL g^{-1}),[70] FMMS (3.4×10^5 mL g^{-1}),[71] and LHMS-1 (9.8×10^6 mL g^{-1}).[64] In short, In_2S_3@MIL-101 could remove 99.95% of Hg from water within 1 min, and this made it an effective and practical adsorbent candidate for potential application. In the meantime, a large-scale synthesized sample can reduce the Hg concentration from 10 ppm down to 1.82 ppb, the removal efficiency of which is almost as equally outstanding as that of the 200 mg scale sample.

As mentioned above, In_2S_3@ MIL-101 has high adsorption capacity and ultrafast kinetics. Such excellent performance may result from the synergistic effect of the large and interconnected cavites of MIL-101 and high affinity of In_2S_3 species toward mercury, where the In_2S_3 nanoparticles provide a large number of sulfur atoms for Hg adsorption and the large cavity of MIL-101 is good for rapid diffusion of Hg. In order to verify such a synergistic effect, we have used pure MIL-101, an In_2S_3 and MIL-101 mixture, and an In_2O_3 and MIL-101 mixture as comparative adsorbents to adsorb Hg under the same conditions. Pure MIL-101 gave a maximum adsorption capacity of about 75 mg g^{-1} when the initial Hg concentration was 1000 mg L^{-1}, much lower than that of In_2S_3@MIL-101 (518.2 mg g^{-1}). Also, 10 mg of MIL-101 only could reduce the concentration of Hg solution from the initial 10 ppm down to 9.21 ppm at pH 7 with an efficiency of 7.9% after 2 h contact, indicating much slower kinetics in comparison to that of In_2S_3@MIL-101 (Figure S7). A 10 mg portion of a In_2S_3/MIL-101 (2.1 mg/7.9 mg) mixture could reduce the concentration of Hg solution from the initial 10 ppm down to 0.92 ppm with an efficiency of 90.8%, while 10 mg of a In_2O_3/MIL-101 (1.9 mg/8.1 mg) mixture only reduced the concentration of Hg solution from the initial 10 ppm down to 9.56 ppm with an efficiency of 4.4% (Figure S8). The results not only show that the sulfur group plays a critical role in the Hg removal process but also indicate that the incorporation of In_2S_3 into MIL-101 is an effective strategy to capture Hg(II) from water.

To further optimize the Hg removal performance, another two In_2S_3@ MIL-101 materials with smaller (0.3 nm) and larger In_2S_3 nanoparticles (2.8 nm) were prepared according to our two-step method by using $In(NO_3)_3$ with initial concentrations of 0.5 and 2 M (Figure S5), respectively. Further research demonstrates that both samples show Hg removal efficiency comparable to that of the title composite (99.98%), in which the removal efficiency of the composite containing smaller nanoparticles is 99.75%, and the composite containing larger nanoparticles shows an efficiency of 99.90% (Figure S9). The results indicate that the size of the nanoparticles has a negligible effect on Hg removal efficiency.

DOI: 10.1021/acs.inorgchem.7b03076
Inorg. Chem. 2018, 57, 4891−4897

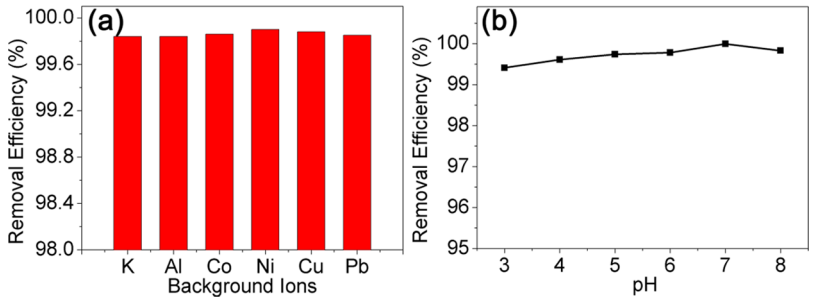

Figure 3. Effects of accompanying different metal ions (a) and pH (b) on the removal of mercury by In_2S_3@MIL-101.

3.4. Effect of Background Ions on Hg Adsorption. Given the existence of interferential metal ions in wastewater, the effect of other metal ions (i.e., K^+, Al^{3+}, Co^{2+}, Ni^{2+}, Cu^{2+}, Pb^{2+}) on the Hg removal efficiency of In_2S_3@MIL-101 was also assessed. As shown in Figure 3a, the Hg removal efficiency for In_2S_3@MIL-101 can be well retained even in the presence of 100 ppm of various background metal ions in the solution when the concentration of Hg is 10 ppm. The good selectivity for Hg was mainly due to the high affinity between Hg and In_2S_3@MIL-101. These studies suggest that In_2S_3@MIL-101 prefers to bind Hg(II) over other interferential ions, highlighting its potential practical use in Hg removal from wastewater.

3.5. Effect of pH on Hg Adsorption. Industrial wastewater is usually acidic, meaning that an adsorbent which has excellent capacity in an acidic environment would be more practical. The pH effect on the adsorption of Hg by In_2S_3@MIL-101 was thus studied in the pH range of 3.0−8.0, as shown in Figure 3b. Notably, the pH value has almost no influence on the removal efficiency for mercury ions. This phenomenon can be interpreted by Pearson's theory that a soft ligand such as an −S group is more easily combined with soft metals such as Hg than with H^+ ion in the solution. The high removal efficiency for Hg by In_2S_3@MIL-101 in an acidic environment should also be potentially important for the removal of Hg from practical industry wastewater.

3.6. Desorption of Hg and Reusability of In_2S_3@MIL-101. Whether In_2S_3@MIL-101 could be regenerated also should be considered a parameter in view of practical application. In_2S_3@MIL-101 can be readily regenerated and recycled by centrifuging after washing the adsorbent with 0.1 M KCl solution and deionized water, respectively. The regenerated In_2S_3@MIL-101 almost retained its original removal efficiency even after three times of regeneration and reuse cycles (Figure S10). The PXRD tests showed that In_2S_3@MIL-101 kept its structure during the reuse cycles (Figure S11). The fine reusability could be attributed to the confinement effect of the MIL-101 framework, which is able to minimize the aggregation of the ultrasmall In_2S_3 NPs.

4. CONCLUSIONS

In conclusion, a facile and rational approach was developed to incorporate ultrasmall In_2S_3 NPs (about 2.5 nm) into the cavities of a representative MOF, MIL-101, for the first time. The resulting composite, In_2S_3@MIL-101, could remove 99.95% of the Hg(II) from wastewater very efficiently within 1 min, achieving the highest distribution coefficient (2.2×10^7 mL g^{-1}) among all MOF-based mercury adsorbents and high saturation adsorption (518.2 mg g^{-1}). In_2S_3@MIL-101 also displayed excellent selectivity for Hg with the presence of other interferential ions exsisted and excellent adsorption capacity in acidic environment, which is very common in practical applications. More importantly, it could be prepared on a large scale and reused with almost retained adsorption capacity. All of the above advantages make In_2S_3@MIL-101 a very promising adsorbent for Hg removal from industrial waste effluents. In short, confinement of ultrasmall metal sulfide nanoparticles in a metal−organic framework indeed provides a convenient and low-cost method for Hg(II) removal. Furthermore, our findings will open new opportunities to synthesize novel hybrid materials based on MOFs for various applications.

■ ASSOCIATED CONTENT

Supporting Information

The Supporting Information is available free of charge on the ACS Publications website at DOI: 10.1021/acs.inorgchem.7b03076.

Detailed information about synthesis and absorption (PDF)

■ AUTHOR INFORMATION

Corresponding Authors

*E-mail for Q.C.: chenqh@fjirsm.ac.cn.
*E-mail for H.-L.J.: jianglab@ustc.edu.cn.
*E-mail for M.H.: hmc@fjirsm.ac.cn.

ORCID

Daqiang Yuan: 0000-0003-4627-072X
Hai-Long Jiang: 0000-0002-2975-7977
Maochun Hong: 0000-0002-1347-6046

Notes

The authors declare no competing financial interest.

■ ACKNOWLEDGMENTS

This paper is dedicated to Professor Xin-Tao Wu on the occasion of his 80th birthday. This work was supported by the "Strategic Priority Research Program" of the Chinese Academy of Sciences (XDB20000000), the 973 Program (2014CB932101), the National Natural Science Foundation of China (21471148, 21731006, 21390392), and the Youth Innovation Promotion Association CAS.

■ REFERENCES

(1) McNutt, M. Mercury and health. *Science* **2013**, *341*, 1430.
(2) Mon, M.; Lloret, F.; Ferrando-Soria, J.; Martí-Gastaldo, C.; Armentano, D.; Pardo, E. Selective and Efficient Removal of Mercury from Aqueous Media with the Highly Flexible Arms of a BioMOF. *Angew. Chem., Int. Ed.* **2016**, *55*, 11167−11172.

DOI: 10.1021/acs.inorgchem.7b03076
Inorg. Chem. 2018, 57, 4891−4897

(3) Lubick, N.; Malakoff, D. With Pact's Completion, The Real Work Begins. *Science* **2013**, *341*, 1443−1445.
(4) Wingenfelder, U.; Hansen, C.; Furrer, G.; Schulin, R. Removal of heavy metals from mine waters by natural zeolites. *Environ. Sci. Technol.* **2005**, *39*, 4606−4613.
(5) Benhammou, A.; Yaacoubi, A.; Nibou, L.; Tanouti, B. Adsorption of metal ions onto Moroccan stevensite: kinetic and isotherm studies. *J. Colloid Interface Sci.* **2005**, *282*, 320−326.
(6) Blanchard, G.; Maunaye, M.; Martin, G. Removal of heavy metals from waters by means of natural zeolites. *Water Res.* **1984**, *18*, 1501−1507.
(7) Huang, C. P.; Blankenship, D. W. The Removal of Mercury(II) from Dilute Aqueous-Solution by Activated Carbon. *Water Res.* **1984**, *18*, 37−46.
(8) Lian, X.; Fang, Y.; Joseph, E.; Wang, Q.; Li, J.; Banerjee, S.; Lollar, C.; Wang, X.; Zhou, H.-C. Enzyme-MOF (metal-organic framework) composites. *Chem. Soc. Rev.* **2017**, *46*, 3386−3401.
(9) Lu, W.; Wei, Z.; Gu, Z.-Y.; Liu, T.-F.; Park, J.; Park, J.; Tian, J.; Zhang, M.; Zhang, Q.; Gentle Iii, T.; Bosch, M.; Zhou, H.-C. Tuning the structure and function of metal-organic frameworks via linker design. *Chem. Soc. Rev.* **2014**, *43*, 5561−5593.
(10) Bosch, M.; Yuan, S.; Rutledge, W.; Zhou, H.-C. Stepwise Synthesis of Metal−Organic Frameworks. *Acc. Chem. Res.* **2017**, *50*, 857−865.
(11) He, H.; Perman, J. A.; Zhu, G.; Ma, S. Metal-Organic Frameworks for CO2 Chemical Transformations. *Small* **2016**, *12*, 6309−6324.
(12) Gao, W. Y.; Chrzanowski, M.; Ma, S. Q. Metal-metalloporphyrin frameworks: a resurging class of functional materials. *Chem. Soc. Rev.* **2014**, *43*, 5841−5866.
(13) Chen, Y.; Ma, S. Q. Biomimetic catalysis of metal-organic frameworks. *Dalton Trans.* **2016**, *45*, 9744−9753.
(14) Kumar, P.; Pournara, A.; Kim, K.-H.; Bansal, V.; Rapti, S.; Manos, M. J. Metal-organic frameworks: Challenges and opportunities for ion-exchange/sorption applications. *Prog. Mater. Sci.* **2017**, *86*, 25−74.
(15) Wang, C.; Zhang, T.; Lin, W. Rational Synthesis of Noncentrosymmetric Metal−Organic Frameworks for Second-Order Nonlinear Optics. *Chem. Rev.* **2012**, *112*, 1084−1104.
(16) Ma, L. Q.; Abney, C.; Lin, W. B. Enantioselective catalysis with homochiral metal-organic frameworks. *Chem. Soc. Rev.* **2009**, *38*, 1248−1256.
(17) Zhu, Q.-L.; Xu, Q. Metal-organic framework composites. *Chem. Soc. Rev.* **2014**, *43*, 5468−5512.
(18) Zhu, Q.-L.; Xu, Q. Immobilization of Ultrafine Metal Nanoparticles to High-Surface-Area Materials and Their Catalytic Applications. *Chem.* **2016**, *1*, 220−245.
(19) O'Keeffe, M.; Yaghi, O. M. Deconstructing the Crystal Structures of Metal−Organic Frameworks and Related Materials into Their Underlying Nets. *Chem. Rev.* **2012**, *112*, 675−702.
(20) Eddaoudi, M.; Sava, D. F.; Eubank, J. F.; Adil, K.; Guillerm, V. Zeolite-like metal-organic frameworks (ZMOFs): design, synthesis, and properties. *Chem. Soc. Rev.* **2015**, *44*, 228−249.
(21) Yan, Y.; Yang, S.; Blake, A. J.; Schröder, M. Studies on Metal−Organic Frameworks of Cu(II) with Isophthalate Linkers for Hydrogen Storage. *Acc. Chem. Res.* **2014**, *47*, 296−307.
(22) Liu, J.; Chen, L.; Cui, H.; Zhang, J.; Zhang, L.; Su, C.-Y. Applications of metal-organic frameworks in heterogeneous supramolecular catalysis. *Chem. Soc. Rev.* **2014**, *43*, 6011−6061.
(23) Zhang, J.-P.; Zhang, Y.-B.; Lin, J.-B.; Chen, X.-M. Metal Azolate Frameworks: From Crystal Engineering to Functional Materials. *Chem. Rev.* **2012**, *112*, 1001−1033.
(24) Wu, H.; Gong, Q.; Olson, D. H.; Li, J. Commensurate Adsorption of Hydrocarbons and Alcohols in Microporous Metal Organic Frameworks. *Chem. Rev.* **2012**, *112*, 836−868.
(25) Sumida, K.; Rogow, D. L.; Mason, J. A.; McDonald, T. M.; Bloch, E. D.; Herm, Z. R.; Bae, T.-H.; Long, J. R. Carbon Dioxide Capture in Metal−Organic Frameworks. *Chem. Rev.* **2012**, *112*, 724−781.
(26) Suh, M. P.; Park, H. J.; Prasad, T. K.; Lim, D.-W. Hydrogen Storage in Metal−Organic Frameworks. *Chem. Rev.* **2012**, *112*, 782−835.
(27) Cui, Y.; Yue, Y.; Qian, G.; Chen, B. Luminescent Functional Metal−Organic Frameworks. *Chem. Rev.* **2012**, *112*, 1126−1162.
(28) Uemura, T.; Yanai, N.; Kitagawa, S. Polymerization reactions in porous coordination polymers. *Chem. Soc. Rev.* **2009**, *38*, 1228−1236.
(29) Ferey, G.; Serre, C. Large breathing effects in three-dimensional porous hybrid matter: facts, analyses, rules and consequences. *Chem. Soc. Rev.* **2009**, *38*, 1380−1399.
(30) Chen, L.; Chen, Q.; Wu, M.; Jiang, F.; Hong, M. Controllable Coordination-Driven Self-Assembly: From Discrete Metallocages to Infinite Cage-Based Frameworks. *Acc. Chem. Res.* **2015**, *48*, 201−210.
(31) Cui, Y.; Li, B.; He, H.; Zhou, W.; Chen, B.; Qian, G. Metal−Organic Frameworks as Platforms for Functional Materials. *Acc. Chem. Res.* **2016**, *49*, 483−493.
(32) Yang, Q.; Xu, Q.; Jiang, H.-L. Metal-organic frameworks meet metal nanoparticles: synergistic effect for enhanced catalysis. *Chem. Soc. Rev.* **2017**, *46*, 4774−4808.
(33) Xie, Z.; Xu, W.; Cui, X.; Wang, Y. Recent Progress in Metal−Organic Frameworks and Their Derived Nanostructures for Energy and Environmental Applications. *ChemSusChem* **2017**, *10*, 1645−1663.
(34) Zhou, X.-P.; Xu, Z.; Zeller, M.; Hunter, A. D. Reversible uptake of $HgCl_2$ in a porous coordination polymer based on the dual functions of carboxylate and thioether. *Chem. Commun.* **2009**, 5439−5441.
(35) Carboni, M.; Abney, C. W.; Liu, S. B.; Lin, W. B. Highly porous and stable metal-organic frameworks for uranium extraction. *Chem. Sci.* **2013**, *4*, 2396−2402.
(36) He, J.; Zha, M.; Cui, J.; Zeller, M.; Hunter, A. D.; Yiu, S.-M.; Lee, S.-T.; Xu, Z. Convenient Detection of Pd(II) by a Metal−Organic Framework with Sulfur and Olefin Functions. *J. Am. Chem. Soc.* **2013**, *135*, 7807−7810.
(37) Zha, M.; Liu, J.; Wong, Y.-L.; Xu, Z. Extraction of palladium from nuclear waste-like acidic solutions by a metal-organic framework with sulfur and alkene functions. *J. Mater. Chem. A* **2015**, *3*, 3928−3934.
(38) Rapti, S.; Sarma, D.; Diamantis, S. A.; Skliri, E.; Armatas, G. S.; Tsipis, A. C.; Hassan, Y. S.; Alkordi, M.; Malliakas, C. D.; Kanatzidis, M. G.; Lazarides, T.; Plakatouras, J. C.; Manos, M. J. All in one porous material: exceptional sorption and selective sensing of hexavalent chromium by using a Zr^{4+} MOF. *J. Mater. Chem. A* **2017**, *5*, 14707−14719.
(39) Rapti, S.; Pournara, A.; Sarma, D.; Papadas, I. T.; Armatas, G. S.; Tsipis, A. C.; Lazarides, T.; Kanatzidis, M. G.; Manos, M. J. Selective capture of hexavalent chromium from an anion-exchange column of metal organic resin-alginic acid composite. *Chem. Sci.* **2016**, *7*, 2427−2436.
(40) Rapti, S.; Pournara, A.; Sarma, D.; Papadas, I. T.; Armatas, G. S.; Hassan, Y. S.; Alkordi, M. H.; Kanatzidis, M. G.; Manos, M. J. Rapid, green and inexpensive synthesis of high quality UiO-66 amino-functionalized materials with exceptional capability for removal of hexavalent chromium from industrial waste. *Inorg. Chem. Front.* **2016**, *3*, 635−644.
(41) Wang, Y.; Ye, G.; Chen, H.; Hu, X.; Niu, Z.; Ma, S. Functionalized metal-organic framework as a new platform for efficient and selective removal of cadmium(ii) from aqueous solution. *J. Mater. Chem. A* **2015**, *3*, 15292−15298.
(42) Tahmasebi, E.; Masoomi, M. Y.; Yamini, Y.; Morsali, A. Application of Mechanosynthesized Azine-Decorated Zinc(II) Metal−Organic Frameworks for Highly Efficient Removal and Extraction of Some Heavy-Metal Ions from Aqueous Samples: A Comparative Study. *Inorg. Chem.* **2015**, *54*, 425−433.
(43) Qi, X.-H.; Du, K.-Z.; Feng, M.-L.; Li, J.-R.; Du, C.-F.; Zhang, B.; Huang, X.-Y. A two-dimensionally microporous thiostannate with superior Cs+ and Sr2+ ion-exchange property. *J. Mater. Chem. A* **2015**, *3*, 5665−5673.
(44) Fang, Q. R.; Yuan, D. Q.; Sculley, J.; Li, J. R.; Han, Z. B.; Zhou, H. C. Functional Mesoporous Metal-Organic Frameworks for the

DOI: 10.1021/acs.inorgchem.7b03076
Inorg. Chem. 2018, 57, 4891−4897

Capture of Heavy Metal Ions and Size-Selective Catalysis. *Inorg. Chem.* **2010**, *49*, 11637−11642.
(45) Yu, C.; Shao, Z.; Hou, H. A functionalized metal-organic framework decorated with O- groups showing excellent performance for lead(ii) removal from aqueous solution. *Chem. Sci.* **2017**, *8*, 7611−7619.
(46) Peng, Y.; Huang, H.; Liu, D.; Zhong, C. Radioactive Barium Ion Trap Based on Metal−Organic Framework for Efficient and Irreversible Removal of Barium from Nuclear Wastewater. *ACS Appl. Mater. Interfaces* **2016**, *8*, 8527−8535.
(47) He, J.; Yee, K.-K.; Xu, Z.; Zeller, M.; Hunter, A. D.; Chui, S. S.-Y.; Che, C.-M. Thioether Side Chains Improve the Stability, Fluorescence, and Metal Uptake of a Metal−Organic Framework. *Chem. Mater.* **2011**, *23*, 2940−2947.
(48) Yee, K.-K.; Reimer, N.; Liu, J.; Cheng, S.-Y.; Yiu, S.-M.; Weber, J.; Stock, N.; Xu, Z. Effective Mercury Sorption by Thiol-Laced Metal−Organic Frameworks: in Strong Acid and the Vapor Phase. *J. Am. Chem. Soc.* **2013**, *135*, 7795−7798.
(49) Liu, T.; Che, J. X.; Hu, Y. Z.; Dong, X. W.; Liu, X. Y.; Che, C. M. Alkenyl/Thiol-Derived Metal-Organic Frameworks (MOFs) by Means of Postsynthetic Modification for Effective Mercury Adsorption. *Chem. - Eur. J.* **2014**, *20*, 14090−14095.
(50) Liang, L.; Chen, Q.; Jiang, F.; Yuan, D.; Qian, J.; Lv, G.; Xue, H.; Liu, L.; Jiang, H.-L.; Hong, M. In situ large-scale construction of sulfur-functionalized metal-organic framework and its efficient removal of Hg(ii) from water. *J. Mater. Chem. A* **2016**, *4*, 15370−15374.
(51) Luo, F.; Chen, J. L.; Dang, L. L.; Zhou, W. N.; Lin, H. L.; Li, J. Q.; Liu, S. J.; Luo, M. B. High-performance Hg^{2+} removal from ultra-low-concentration aqueous solution using both acylamide- and hydroxyl-functionalized metal-organic framework. *J. Mater. Chem. A* **2015**, *3*, 9616−9620.
(52) Hou, Y.-L.; Yee, K.-K.; Wong, Y.-L.; Zha, M.; He, J.; Zeller, M.; Hunter, A. D.; Yang, K.; Xu, Z. Metalation Triggers Single Crystalline Order in a Porous Solid. *J. Am. Chem. Soc.* **2016**, *138*, 14852−14855.
(53) Rudd, N. D.; Wang, H.; Fuentes-Fernandez, E. M. A.; Teat, S. J.; Chen, F.; Hall, G.; Chabal, Y. J.; Li, J. Highly Efficient Luminescent Metal−Organic Framework for the Simultaneous Detection and Removal of Heavy Metals from Water. *ACS Appl. Mater. Interfaces* **2016**, *8*, 30294−30303.
(54) Férey, G.; Mellot-Draznieks, C.; Serre, C.; Millange, F.; Dutour, J.; Surblé, S.; Margiolaki, I. A Chromium Terephthalate-Based Solid with Unusually Large Pore Volumes and Surface Area. *Science* **2005**, *309*, 2040−2042.
(55) Aijaz, A.; Karkamkar, A.; Choi, Y. J.; Tsumori, N.; Ronnebro, E.; Autrey, T.; Shioyama, H.; Xu, Q. Immobilizing highly catalytically active Pt nanoparticles inside the pores of metal-organic framework: a double solvents approach. *J. Am. Chem. Soc.* **2012**, *134*, 13926−13929.
(56) Oubagaranadin, J. U. K.; Sathyamurthy, N.; Murthy, Z. V. P. Evaluation of Fuller's earth for the adsorption of mercury from aqueous solutions: A comparative study with activated carbon. *J. Hazard. Mater.* **2007**, *142*, 165−174.
(57) Tuzen, M.; Sari, A.; Mendil, D.; Soylak, M. Biosorptive removal of mercury(II) from aqueous solution using lichen (Xanthoparmelia conspersa) biomass: Kinetic and equilibrium studies. *J. Hazard. Mater.* **2009**, *169*, 263−270.
(58) Boparai, H. K.; Joseph, M.; O'Carroll, D. M. Kinetics and thermodynamics of cadmium ion removal by adsorption onto nano zerovalent iron particles. *J. Hazard. Mater.* **2011**, *186*, 458−465.
(59) Febrianto, J.; Kosasih, A. N.; Sunarso, J.; Ju, Y.-H.; Indraswati, N.; Ismadji, S. Equilibrium and kinetic studies in adsorption of heavy metals using biosorbent: A summary of recent studies. *J. Hazard. Mater.* **2009**, *162*, 616−645.
(60) Ke, F.; Qiu, L. G.; Yuan, Y. P.; Peng, F. M.; Jiang, X.; Xie, A. J.; Shen, Y. H.; Zhu, J. F. Thiol-functionalization of metal-organic framework by a facile coordination-based postsynthetic strategy and enhanced removal of Hg^{2+} from water. *J. Hazard. Mater.* **2011**, *196*, 36−43.
(61) Huang, L.; He, M.; Chen, B.; Hu, B. A mercapto functionalized magnetic Zr-MOF by solvent-assisted ligand exchange for Hg^{2+} removal from water. *J. Mater. Chem. A* **2016**, *4*, 5159−5166.
(62) Huang, L.; He, M.; Chen, B.; Hu, B. A designable magnetic MOF composite and facile coordination-based post-synthetic strategy for the enhanced removal of Hg^{2+} from water. *J. Mater. Chem. A* **2015**, *3*, 11587−11595.
(63) Manos, M. J.; Kanatzidis, M. G. Sequestration of Heavy Metals from Water with Layered Metal Sulfides. *Chem. - Eur. J.* **2009**, *15*, 4779−4784.
(64) Manos, M. J.; Petkov, V. G.; Kanatzidis, M. G. $H_{2x}Mn_xSn_{3-x}S_6$ (x = 0.11−0.25): A Novel Reusable Sorbent for Highly Specific Mercury Capture Under Extreme pH Conditions. *Adv. Funct. Mater.* **2009**, *19*, 1087−1092.
(65) Rostamian, R.; Najafi, M.; Rafati, A. A. Synthesis and characterization of thiol-functionalized silica nano hollow sphere as a novel adsorbent for removal of poisonous heavy metal ions from water: Kinetics, isotherms and error analysis. *Chem. Eng. J.* **2011**, *171*, 1004−1011.
(66) Wang, M.; Qu, R.; Sun, C.; Yin, P.; Chen, H. Dynamic adsorption behavior and mechanism of transition metal ions on silica gels functionalized with hydroxyl- or amino-terminated polyamines. *Chem. Eng. J.* **2013**, *221*, 264−274.
(67) Qu, R.; Zhang, Y.; Sun, C.; Wang, C.; Ji, C.; Chen, H.; Yin, P. Adsorption of Hg(II) from an Aqueous Solution by Silica-Gel Supported Diethylenetriamine Prepared via Different Routes: Kinetics, Thermodynamics, and Isotherms. *J. Chem. Eng. Data* **2010**, *55*, 1496−1504.
(68) Li, B.; Zhang, Y.; Ma, D.; Shi, Z.; Ma, S. Mercury nano-trap for effective and efficient removal of mercury(II) from aqueous solution. *Nat. Commun.* **2014**, *5*, 5537.
(69) Huang, N.; Zhai, L.; Xu, H.; Jiang, D. Stable Covalent Organic Frameworks for Exceptional Mercury Removal from Aqueous Solutions. *J. Am. Chem. Soc.* **2017**, *139*, 2428−2434.
(70) Shin, Y.; Fryxell, G. E.; Um, W.; Parker, K.; Mattigod, S. V.; Skaggs, R. Sulfur-Functionalized Mesoporous Carbon. *Adv. Funct. Mater.* **2007**, *17*, 2897−2901.
(71) Feng, X.; Fryxell, G. E.; Wang, L.-Q.; Kim, A. Y.; Liu, J.; Kemner, K. M. Functionalized Monolayers on Ordered Mesoporous Supports. *Science* **1997**, *276*, 923−926.

DOI: 10.1021/acs.inorgchem.7b03076
Inorg. Chem. 2018, 57, 4891−4897